IOP Publishing Nanotechnology
Nanotechnology 27 (2016) 425710 (8pp) doi:10.1088/0957-4484/27/42/425710

Size dependence of phosphorus doping in silicon nanocrystals

Wei He[1,2], Zhengping Li[1], Chao Wen[1], Hong Liu[1] and Wenzhong Shen[1]

[1] Laboratory of Condensed Matter Spectroscopy and Opto-Electronic Physics, Key Laboratory of Artificial Structures and Quantum Control (Ministry of Education), Institute of Solar Energy, Department of Physics and Astronomy, Shanghai Jiao Tong University, Shanghai 200240, People's Republic of China
[2] School of New Energy Science and Engineering, Xinyu Institute of New Energy, Xinyu University, Xinyu 338004, People's Republic of China

E-mail: zpli@sjtu.edu.cn and wzshen@sjtu.edu.cn

Received 25 March 2016, revised 27 June 2016
Accepted for publication 11 July 2016
Published 15 September 2016

Abstract

Doping of silicon nanocrystals (Si-NCs) is one of the major challenges for silicon nanoscale devices. In this work, phosphorus (P) doping in Si-NCs which are embedded within an amorphous silicon matrix is realized together with the growth of Si-NCs by plasma-enhanced chemical vapor deposition under a tunable substrate direct current (DC) bias. The variation of phosphorus concentration with substrate bias can be explained by the competition of bonding processes of Si–Si and P–Si bonds. The formation of Si–Si and P–Si bonds is differently influenced by the ion bombardment controlled by the substrate bias, due to their bonding energy difference. We have studied the influences of grain size on P doping in Si-NCs. Free carrier concentration, which is provided by activated P atoms, decreases with decreasing grain size due to increasing formation energy and activation energy of P atoms incorporated in Si-NCs. Furthermore, we have studied the P locations inside Si-NCs and hydrogen passivation of P in the form of P–Si–H complexes using the first-principles method. Hydrogen passivation of P can also contribute to the reduced free carrier concentration in smaller Si-NCs. These results provide valuable understanding of P doping in Si-NCs.

Keywords: phosphorus doping, silicon nanocrystals, negative DC bias, formation energy, activation energy, hydrogen passivation

1. Introduction

Doping of silicon is crucial to the rapid development of the semiconductor industry. Typical dopant atoms such as phosphorus (P) and boron in crystalline silicon are in fourfold coordinated substitutional sites as shallow level impurities, and can be easily ionized at room temperature, leading to almost 100% doping efficiency. However, with the successive development of integrated opto-electronic devices, as the feature size shrinks to nanoscale, the doping process becomes more difficult [1–5]. For instance, the doping efficiency of P in freestanding silicon nanocrystals (Si-NCs) has been found to significantly decrease with decreasing grain size, which was attributed to charge compensation of interface dangling bonds, according to the work of Stegner *et al* [6]. Moreover, P has been found to be difficult to ionize in Si-NCs because the P donor level becomes deeper in them [5, 7].

To resolve this problem, more detailed mechanisms of the dopant behavior in the Si-NCs need to be understood. As is well known, incorporation and activation of P atoms are two primary processes in the P doping of Si-NCs, which are mainly determined by formation energy and activation energy, respectively [1]. The decrease of P doping efficiency and harder ionization in Si-NCs have been predicted by first-principles calculations which related them to increasing formation energy and activation energy of a single dopant atom in nanocrystals with decreasing grain size [1–4]. To further experimentally explore the mechanisms, systematic experiments should be performed. We employ the system of P-doped hydrogenated nanocrystalline silicon (nc-Si:H), a mixed-phase structure of Si-NCs embedded in an amorphous silicon matrix, produced by plasma enhanced chemical vapor deposition (PECVD). Previous research [8] has shown that applying a negative direct current (DC) bias on the substrate

is an effective technique to alter the kinetic energy of the ions during PECVD, which can strongly influence the ion bombardment on the growing surface. Thus, phosphorus concentration would be controlled by selectively etching of Si-Si bonds under a tunable negative DC bias applied on the substrate during the deposition process, since the Si-Si bonding energy is relatively smaller than the P-Si bonding energy [9]. Meanwhile, owing to the comprehensive effect of ion bombardment-induced amorphization [10, 11], hydrogen-induced annealing [12, 13] and dopant atom-induced local deformation [14, 15], grain size of the Si-NCs can also be regulated by the negative DC bias. Therefore, the P-doped nc-Si:H prepared under a tunable negative DC bias is suitable for studying the size dependence of phosphorus doping in Si-NCs.

In this work, atomic phosphorus concentration [P] of nc-Si:H was tuned by varying the substrate DC bias with constant feed gas ratio ($[PH_3]/[SiH_4]$) and hydrogen dilution ratio ($[H_2]/([H_2] + [SiH_4])$) in PECVD. Experimental results from secondary ion mass spectrometry (SIMS), x-ray photoelectron spectroscopy (XPS) and x-ray diffraction (XRD) spectra demonstrated that [P] was enhanced with decreasing grain size. Nevertheless, free carrier concentration, i.e., effective doping efficiency, yielded from Hall effect measurements, was found to decrease with decreasing grain size. We performed *ab initio* first-principles calculations on spherical $Si_{47}H_{60}$-based Si-NCs (approximately 1.2 nm in diameter) doped with single P atom to study P locations inside Si-NCs and hydrogen passivation of P. Results from Fourier transform infrared (FTIR) absorption spectra showed good agreement with the theoretical analyses. We manifested that the size dependence of P doping in Si-NCs was mainly associated with formation energy, activation energy and hydrogen passivation.

2. Experimental details

The P-doped nc-Si:H films were deposited on both glass (Corning 7059) and double side polished intrinsic crystalline silicon (100) substrates at temperature of 250 °C by a PECVD system with radio frequency of 13.56 MHz and power density of 0.4 W cm^{-2}. The reactive gases were a mixture of SiH_4, H_2 and PH_3 with total gas flow rate of 120 sccm and chamber pressure of 150 Pa. The hydrogen dilution ratio ($[H_2]/([H_2] + [SiH_4])$) and feed gas ratio ($[PH_3]/([PH_3] + [SiH_4])$) were fixed at 99% and 10%, respectively. A negative DC bias ranging from 0 V to −300 V was applied to the stainless steel substrate holder.

The average grain size d was derived from XRD spectra, measured with a Goniometer Ultima IV diffractometer (Cu Kα radiation, 40 kV and 30 mA). Raman spectra were obtained by a Jobin Yvon LabRam HR800 UV micro-Raman spectrometer (backscattering configuration and Ar ion laser at a wavelength of 514.5 nm). Optical transmission spectra were measured in 300 ∼ 1000 nm spectral range by a double-beam ultraviolet-visible-near infrared spectrometer (PerkinElmer UV Lambda 35), from which the optical band gap E_g was deduced using Tauc's linear extrapolation method [16, 17]. The atomic concentrations of phosphorus, hydrogen and oxygen were analyzed by SIMS analysis in a Cameca IMS-7f apparatus using 9 kV Cs primary ions (detection angle of 23° and ion intensity of 30 nA). P 2p, O 1s and Si 2p photoelectron spectra were collected by XPS measurements in an AXIS UltraDLD system with an Al Kα source monochromatic x-ray radiation at an emission angle of 90°. The binding energy was calibrated with C 1s emission energy at 284.8 eV. The electronic transport properties such as carrier concentration, carrier mobility and conductivity were measured by a Hall effect measurement system (ECOPIA HMS 5300). The bonded-hydrogen content C_H, bonded-oxygen content C_O, and their bonding configurations were obtained by infrared absorption spectra from 400 cm^{-1} to 4000 cm^{-1} using a Nicolet Nexus 870 FTIR spectrometer. The thicknesses of the films were obtained by a KLA-Tencor P-7 Profiler, which were approximately 500 nm. All the measurements were performed at room temperature.

3. Theoretical treatment

A model of spherical nanocrystal, undoped $Si_{47}H_{60}$ with 1.2 nm-diameter, was constructed by cutting out a spherical portion in an optimized bulk Si model and passivating the surface dangling bonds with H atoms. We carried out *ab initio* first-principles calculations to study the electronic properties of $Si_{47}H_{60}$-based nanocrystals doped with single P atom. We discussed the relative energetic stability of Si-NCs with single P atom in different substitutional sites, and compared the electronic properties among undoped, P-doped and H-passivated Si-NCs to investigate the hydrogen passivation of P. In the calculation, a linear combination of the atomic orbitals technique [18, 19] was employed to study the electronic structure of Si-NCs. Double numerical basis sets augmented with p-polarization functions were adopted as the atomic orbit basis functions. Becke–Lee–Yang–Parr correlation exchange functional [20] at the generalized gradient approximation level was used. To ensure calculation accuracy, a high self-consistent field convergence threshold was set to 10^{-6}. The maximum forces, displacement and energy on all of the atoms in the optimized structures were less than 0.002 Ha/Å, 0.005 Å and 10^{-5} Ha/atom, respectively. The k-points for the Brillouin-zone sampling were set as Gamma point only for all cases.

4. Results and discussion

We performed XRD and Raman measurements to obtain the structural properties of the nc-Si:H films prepared under various substrate DC biases. Figure 1(a) presents the XRD pattern of a typical sample under −100 V DC bias. The diffraction peaks at $2\theta \approx 28.3°$, 47.4° and 55.7° correspond to (111), (220) and (311) planes of crystalline silicon, respectively. The Si-NCs have shown preferential growth direction along the (111) crystal orientation, as seen from figure 1(a)

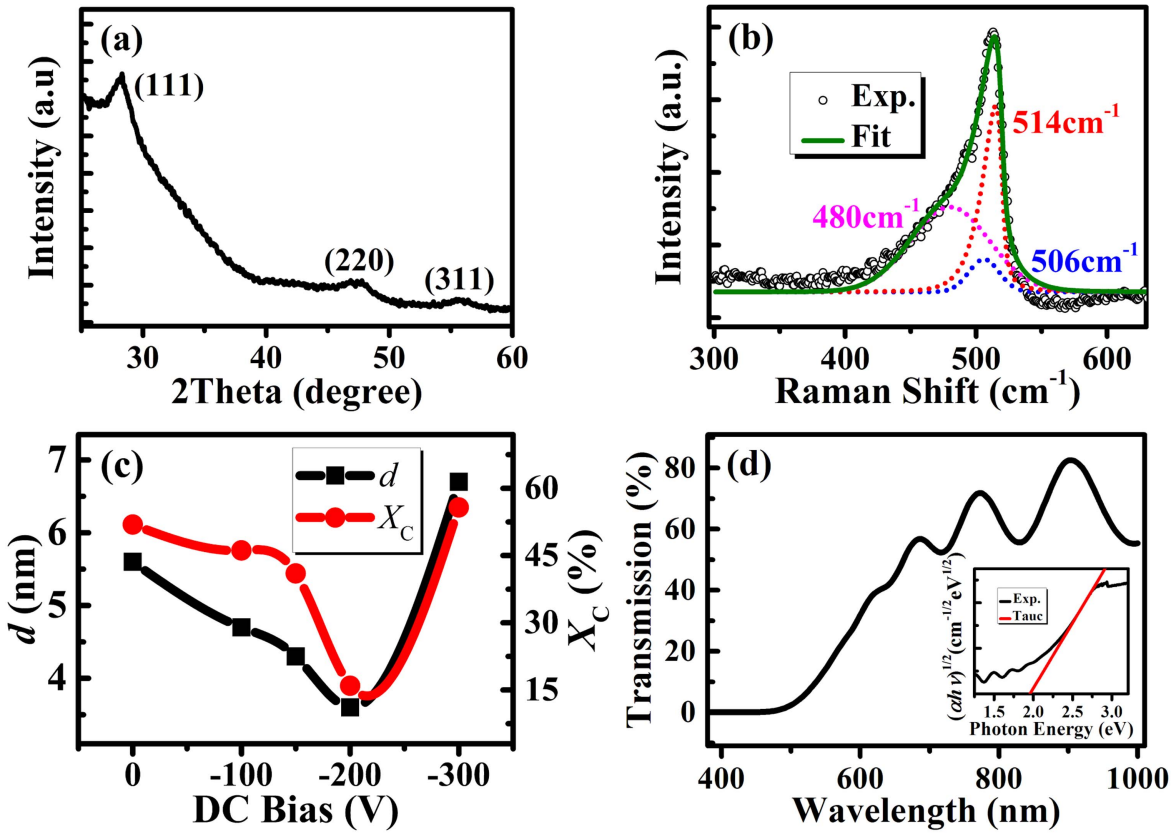

Figure 1. Structural and optical properties of a representative nc-Si:H sample under −100 V DC bias. (a) Experimental XRD spectrum showing diffraction peaks (111), (220) and (311). (b) Experimental (open circles) and fitted Raman spectrum. (c) Average grain sizes d and crystalline volume fractions X_C of the samples under various DC biases. (d) Experimental optical transmission spectrum with Tauc-plot shown in the inset. Solid lines in (c) are a guide to the eye.

that the intensity of the (111) peak is the strongest and sharpest among the three peaks. Compared with crystalline silicon, broadening of the three peaks indicates that the Si-NCs are embedded in an amorphous silicon matrix. The average grain size d can be calculated from the (111) crystal orientation of the XRD pattern using the well-known Scherrer formula [21]: $d = k\lambda/(\beta\cos\theta)$, where $k = 0.94$ is a constant, $\lambda = 0.154$ nm is the wavelength of the x-ray, β is the full width at half-maximum of the diffraction peak, and θ is the Bragg angle. Figure 1(b) shows the Raman spectrum of the sample under −100 V DC bias. The spectrum can be decomposed into three independent Gaussian components [22, 23]: a narrow peak near 520 cm^{-1}, which belongs to the asymmetric transverse optical mode of crystalline silicon, an intermediate mode of crystal-like phase around 506 cm^{-1} attributed to Si-Si bond dilation at grain boundaries, and a broad peak at 480 cm^{-1}, which originates from the transverse optical mode of amorphous silicon. Furthermore, the crystalline volume fraction X_C can be calculated from the formula [22, 23]: $X_C = (I_C + I_{GB})/(I_C + I_{GB} + I_A)$, where I_C, I_{GB} and I_A represent integrated intensities of the crystalline phase, grain boundary phase and amorphous phase, respectively. As shown in figure 1(c), it could be clearly seen that the grain size d decreases from 5.6 nm to 3.6 nm when the DC bias increases from 0 V to −200 V, then increases to 6.7 nm when the DC bias further increases to −300 V. The change of crystalline volume fraction X_C with DC bias is similar to that of grain size, which is also depicted in figure 1(c). Figure 1(d) displays the optical transmission spectra for the sample under −100 V DC bias. According to Tauc's linear extrapolation method [16, 17], the optical band gap E_g (1.96 eV) can be deduced from the following formula: $(\alpha h\nu)^{0.5} = B_a(h\nu - E_g)$, where α is absorption coefficient, $h\nu$ is photon energy and B_a is a constant, as shown in the inset of figure 1(d).

With the increasing DC bias, positive ionic species in plasmas gain a higher kinetic energy due to the acceleration of the DC electric field. In the initial increasing stage of the DC bias from 0 V to −200 V, more distorted chemical bonds are formed on the growing surface under bombardment of the positive ionic species. Thus, amorphous phase content will increase, corresponding to the decrease of grain size and crystalline volume fraction, as illustrated in figure 1(c). It can be ascribed to the ion bombardment-induced amorphization [10, 11] in the DC bias range. While further increasing the DC bias to −300 V, the H atoms and ions on the growing surface are energetic enough to permeate into the subsurface and rearrange the amorphous silicon network structure. The H atoms and ions insert into the strained Si-Si bonds, and subsequent relaxation of the structure leads to the transformation of amorphous silicon to nanocrystalline silicon. Therefore, the grain size and crystalline volume fraction

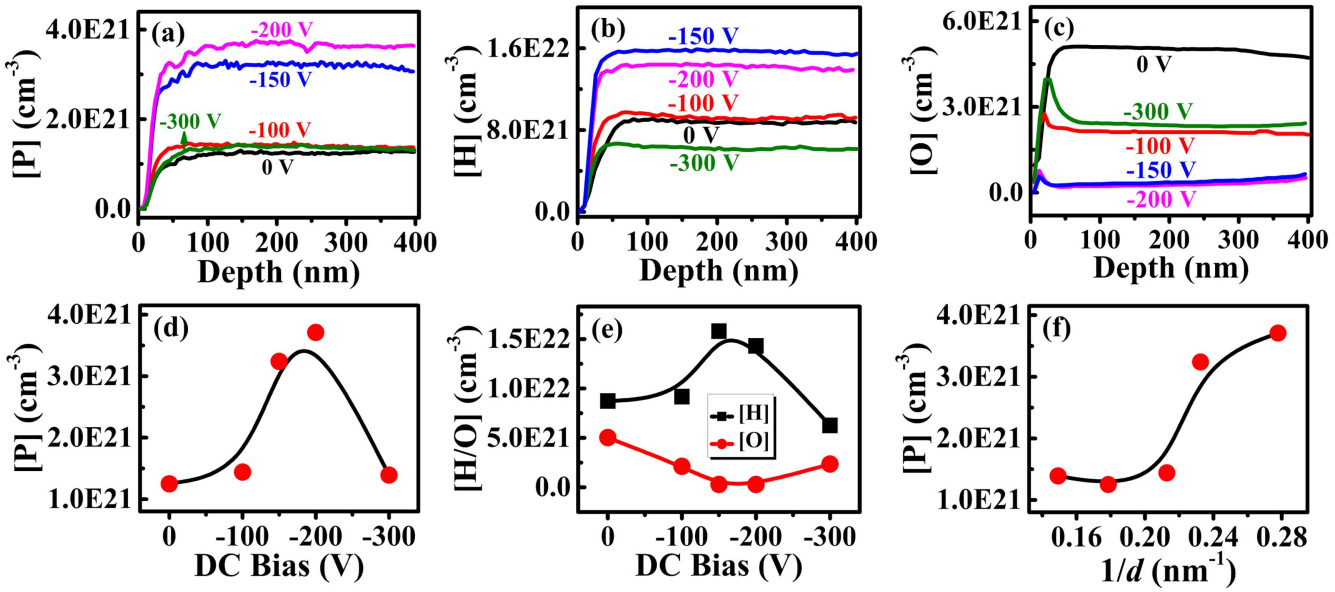

Figure 2. Atomic concentrations of (a) P, (b) H and (c) O as a function of depth under various DC biases obtained by SIMS. Atomic concentrations of (d) P, (e) H and O at the depth of 200 nm as a function of DC bias. (f) Atomic concentration of P at the depth of 200 nm as a function of inverse grain size $1/d$. Solid lines in (d), (e) and (f) are a guide to the eye.

increase due to the hydrogen-induced annealing effect [12, 13] in the DC bias range of $-200 \sim -300$ V, as shown in figure 1(c). In contrast to our previous study on intrinsic nc-Si:H films [8], the grain size and crystalline volume fraction display a similar but more obvious change due to the additional P-induced local deformation, which we will elucidate later.

In order to study the elemental distribution in the nc-Si:H films, we measure the phosphorus, hydrogen and oxygen concentrations in the samples directly by SIMS. Figures 2(a)–(c) present the atomic concentrations of phosphorus [P], hydrogen [H] and oxygen [O] as a function of depth under various DC biases, respectively. We can see that the three elements concentrations are nearly constant under each DC bias in the region of the plateau between 100 nm and 400 nm. Thus, we plot the three elements concentrations at the depth of 200 nm as a function of DC bias, as shown in figures 2(d) and (e). It can be seen that [P] increases as the DC bias increases from 0 V to -200 V, and then decreases as the DC bias further increases to -300 V. There is a negative correlation between [H] and [O], which could be interpreted by the hydrogen passivation of dangling bonds [24]. Due to the incorporation of hydrogen atoms with the silicon dangling bonds located at grain boundaries, less oxygen atoms could reside along grain boundaries in the form of Si–O bond.

There are two competing processes during which phosphorus and silicon atoms are incorporated into nc-Si:H films. The first one is absorption of phosphorus and silicon atoms from the plasmas through bonding between radicals, molecules and growing surface. The second one is desorption of phosphorus and silicon atoms from the growing surface through etching of P–Si and Si–Si bonds. With the increasing DC bias, positive ionic species will gain a higher kinetic energy and bombard the growing surface more severely, resulting in selectively etching of Si–Si bonds since the Si–Si bonding energy (321 kJ mol^{-1}) is relatively smaller than the P–Si bonding energy (331 kJ mol^{-1}) [9]. Under the bombardment of the positive ionic species, a part of kinetic energy of these species is transferred to P and Si atoms on the growing surface. Thus, the corresponding P–Si and Si–Si bonds will break more easily. In the initial increasing stage of the DC bias ($0 \sim -200$ V), P–Si and Si–Si bonds will be etched simultaneously, but more P–Si bonds will remain due to the larger bonding energy, which can be evidenced by the fact that [P] increases obviously from 1.25×10^{21} cm^{-3} to 3.71×10^{21} cm^{-3} in figure 2(d). However, further increasing the DC bias to -300 V, kinetic energy of the positive ionic species is enhanced so much that P–Si bonds will also be etched severely. Consequently, [P] decreases to 1.39×10^{21} cm^{-3}, as shown in figure 2(d). It is worthwhile to note that phosphorus concentration varies inversely with grain size, as shown in figure 2(f). Since the P–Si bond is shorter than the Si–Si bond [25], local deformation will be induced by phosphorus incorporation. A higher phosphorus concentration in the nc-Si:H films will reduce the tendency toward crystallization, which is in agreement with previous observation [15].

We have also employed XPS measurements to obtain the chemical composition of the P-doped nc-Si:H films. There are two peaks centered at around 128.9 eV and 133.8 eV in the P 2p spectra of figure 3(a) corresponding to the P–Si bond and P–O bond, respectively [26]. It is clearly seen that the P–Si bond of the sample under -200 V DC bias is the most prominent, which indicates that phosphorus concentration of the sample is the highest among the five samples. This is in perfect agreement with the SIMS data in figure 2(d). From figure 3(b), we can see that there exists a peak at around 532.3 eV in the O 1s spectra, corresponding to the Si–O bond

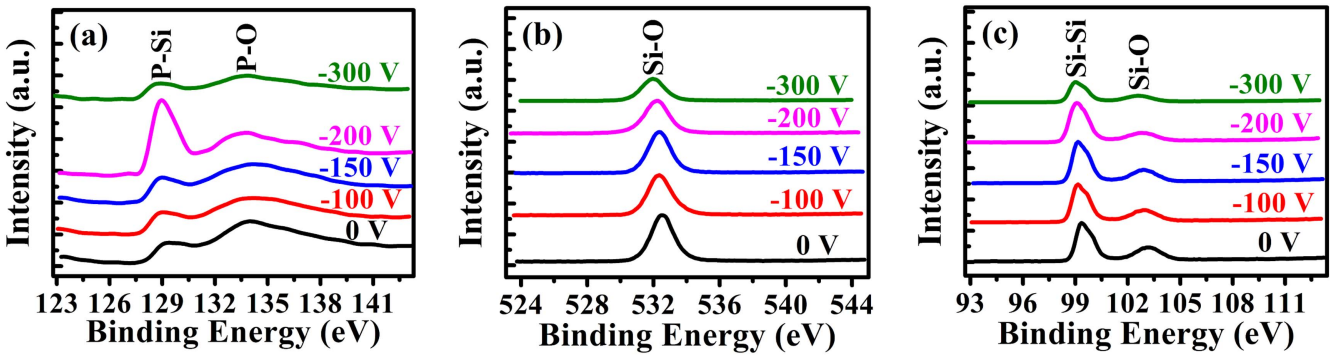

Figure 3. XPS spectra of (a) P 2p, (b) O 1s and (c) Si 2p for the samples under various DC biases.

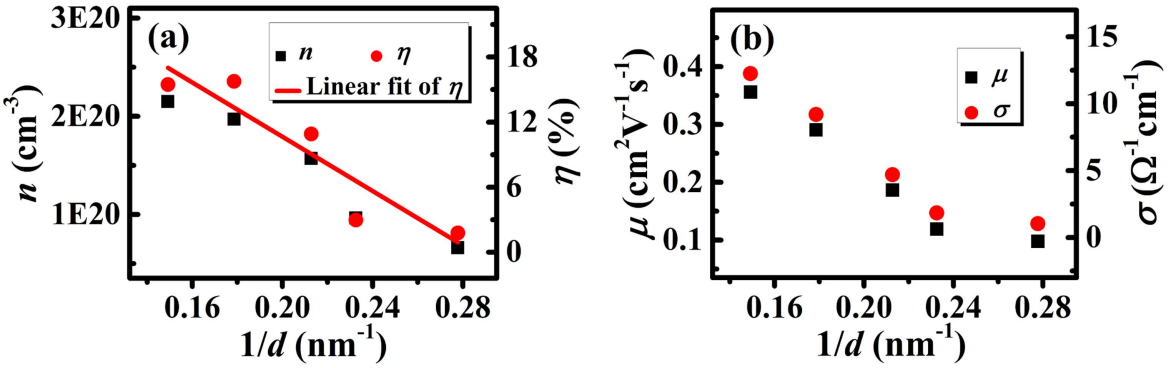

Figure 4. (a) Free carrier concentration n and effective doping efficiency η as a function of inverse grain size $1/d$. (b) Carrier mobility μ and conductivity σ as a function of inverse grain size $1/d$.

[27]. As shown in figure 3(c), the Si 2p spectra present two peaks located at about 99.1 eV and 102.9 eV, corresponding to the Si^0 state (Si–Si bond) and Si^{4+} state (Si–O bond), respectively [26, 28]. The intensity of the Si–O bond decreases monotonously with increasing DC bias from 0 V to −300 V in both figures 3(b) and (c), indicating that oxygen concentration on the surface decreases along with increasing DC bias. However, it is somewhat different from that obtained by SIMS measurements in figure 2(e). The difference may be related to the surface smoothness at the atomic level of the sample, i.e., a rough surface of the sample produces more intermediate oxidation states [28]. The oxygen concentration in the bulk is mainly influenced by hydrogen concentration and hydrogen-related defect structure [24].

In order to further investigate the activation of the incorporated P atoms in Si-NCs, we carried out Hall effect measurements for the electronic transport properties of the nc-Si:H films. Effective doping efficiency $\eta = n/[\mathrm{P}]$ is defined to evaluate ratio of free carrier concentration to total dopant atom concentration [29], where n is a free carrier (electron) concentration obtained by Hall effect measurements. Figure 4 presents the variations of free carrier concentration n, effective doping efficiency η, carrier mobility μ and conductivity σ as a function of inverse grain size $1/d$. It could be clearly seen that all these quantities decrease as the grain size decreases. The P atoms incorporated in nc-Si:H films may locate in nanocrystals and amorphous matrix. According to first-principles calculation results [1], the formation energy of P atoms incorporated in Si-NCs increases with decreasing grain size. It becomes more difficult to dope Si-NCs with smaller grain size, and consequently, more P atoms would be incorporated in amorphous matrix. Moreover, first-principles calculation results [1] indicate that the activation energy of P atoms incorporated in Si-NCs is a decreasing function of grain size. Thus, it would be more difficult to electrically activate P atoms for smaller nanocrystals. Therefore, free carrier concentration and effective doping efficiency decrease as the grain size decreases.

We have also performed *ab initio* first-principles calculations on P location inside Si-NCs and hydrogen passivation of P to get deeper understanding on P doping in Si-NCs. As shown in figure 5(a), there are six different substitutional sites for P substitution of Si in the nanocrystal, which are labeled as 1 to 6 from center to surface, respectively. These sites are classified into three groups: sites 1 and 2 in the core of the nanocrystal, sites 4, 5 and 6 in the surface layer of the nanocrystal, and site 3 in the subsurface layer of the nanocrystal. The relative energetic stability of these P-doped Si-NCs can be evaluated by comparing the formation energy E_f. Starting from the undoped Si_nH_m nanocrystal, the formation energy for single P atom is calculated from the formula [1]: $E_f = E(Si_{n-1}PH_m) - E(Si_nH_m) + \mu_{Si}\text{-}\mu_P$, where $E(Si_{n-1}PH_m)$ is the total energy of the P-doped system, $E(Si_nH_m)$ is the total energy of the undoped system, μ_{Si} is the total energy per atom of bulk Si, and μ_P is the total energy per atom of P. Although μ_{Si} and μ_P depend on the specific experimental

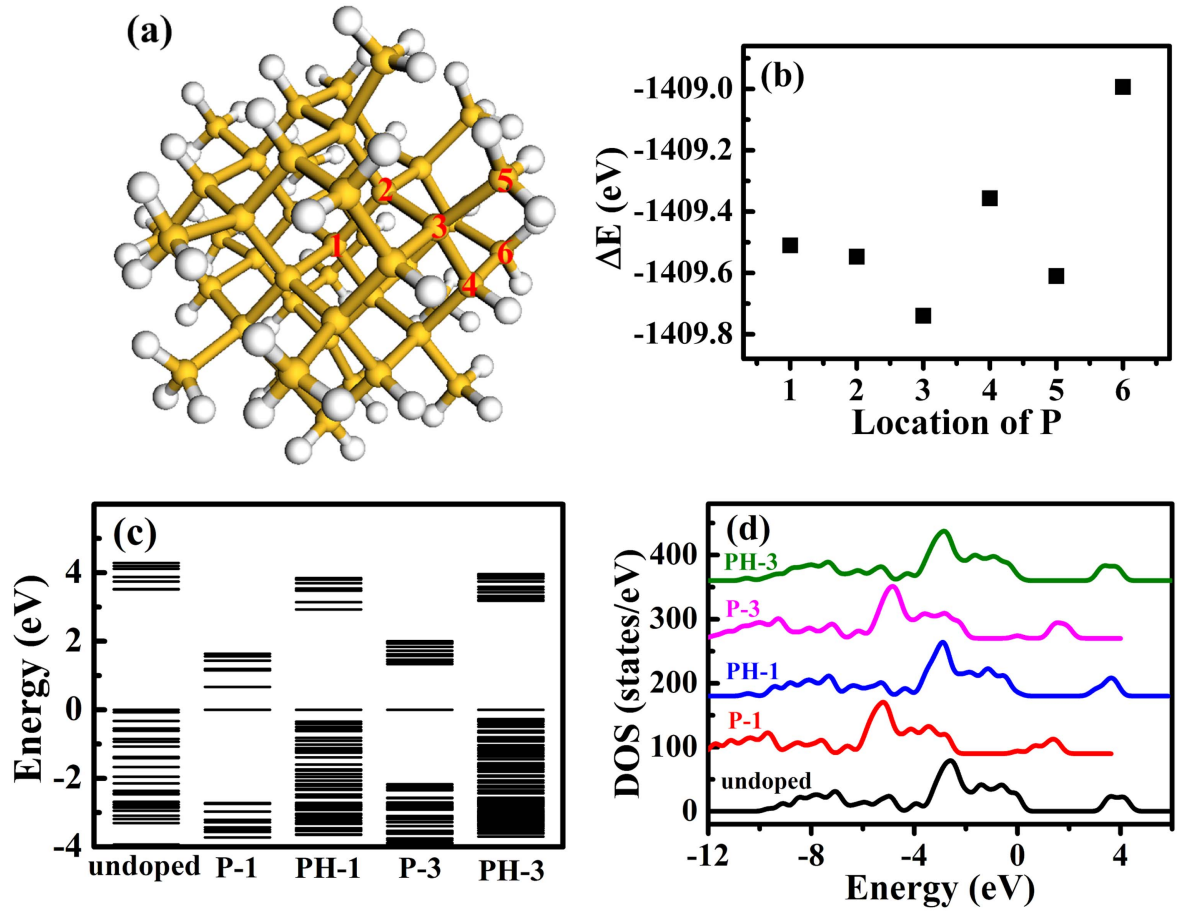

Figure 5. (a) Model of $Si_{47}H_{60}$ nanocrystal. Si and H atoms are denoted by yellow and white balls, respectively. Six different substitutional sites for P substitution of Si are labeled as 1 to 6 from center to surface, respectively. (b) Difference of total energy between P-doped and undoped Si-NCs, ΔE, as a function of P location. (c) Band structure and (d) electronic densities of state (DOS) for undoped, P-doped and H-passivated $Si_{47}H_{60}$-based nanocrystals. The labels undoped, P-1, PH-1, P-3, PH-3 in (c) and (d) denote undoped case, P doping at site 1, H passivating P at site 1, P doping at site 3, H passivating P at site 3, respectively.

conditions, they can be deemed as constants under the same experimental conditions. As a result, the difference between $E(Si_{n-1}PH_m)$ and $E(Si_nH_m)$, ΔE, evaluates the relative energetic stability of these P-doped Si-NCs. Figure 5(b) illustrates the calculated ΔE as a function of P location. It is found that the value of ΔE at site 3 is minimum, which is 0.23 eV lower than that at site 1. In addition, the value of ΔE at site 5 is the second-lowest, which is 0.13 eV above the minimum value. Such calculation results indicate that sites 3 and 5 are energetically the most favorable for P substitution of Si. Hence, most of the P atoms incorporated in Si-NCs prefer to reside near the surface of the nanocrystals. Similar experimental observations have been reported in colloidal Si-NCs [6, 30].

Calculation on hydrogen passivation of P has been further conducted at sites 1 and 3 of the $Si_{47}H_{60}$ nanocrystal. The passivating H atom is located at the antibonding site of a Si atom bonded to the substitutional P, forming P-Si-H complex, which was found to be the minimum-energy configuration by Johnson *et al* [31] and Chang *et al* [32]. The calculated band structure and electronic densities of state (DOS) for undoped, P-doped and H-passivated $Si_{47}H_{60}$-based nanocrystals are depicted in figures 5(c) and (d). The band structure and DOS of H-passivated Si-NCs are similar to those of undoped Si-NCs, though the bandgap of H-passivated Si-NCs is a bit smaller than that of undoped Si-NCs. Compared with undoped case, P doping introduces impurity energy levels and new electronic states in the forbidden band. However, after hydrogen passivation of P, such impurity energy levels and electronic states disappear. In other words, H can indeed passivate P atoms in the form of P-Si-H complex in Si-NCs, resulting in reduced free carrier concentration, i.e., the P-Si-H complex in Si-NCs behaves similarly to that in crystalline Si and Si nanowires [31–34]. It is worthwhile to note that the impurity energy level introduced by P at site 3 is much deeper than that at site 1, demonstrating that P atoms incorporated near the surface of the nanocrystal are more difficult to be electrically activated than those incorporated in the core of the nanocrystal.

Finally, the FTIR absorption spectra have been performed to investigate hydrogen passivation of P. As shown in figure 6(a), there are four absorption peaks appearing in the infrared spectra, which are Si-H rocking/wagging mode at around 640 cm^{-1}, Si-H bending mode at around 880 cm^{-1}, Si-H stretching mode at around 2090 cm^{-1}, and Si-O stretching mode at around 1070 cm^{-1} [35–38]. The bonded-hydrogen content C_H could be calculated by numerical

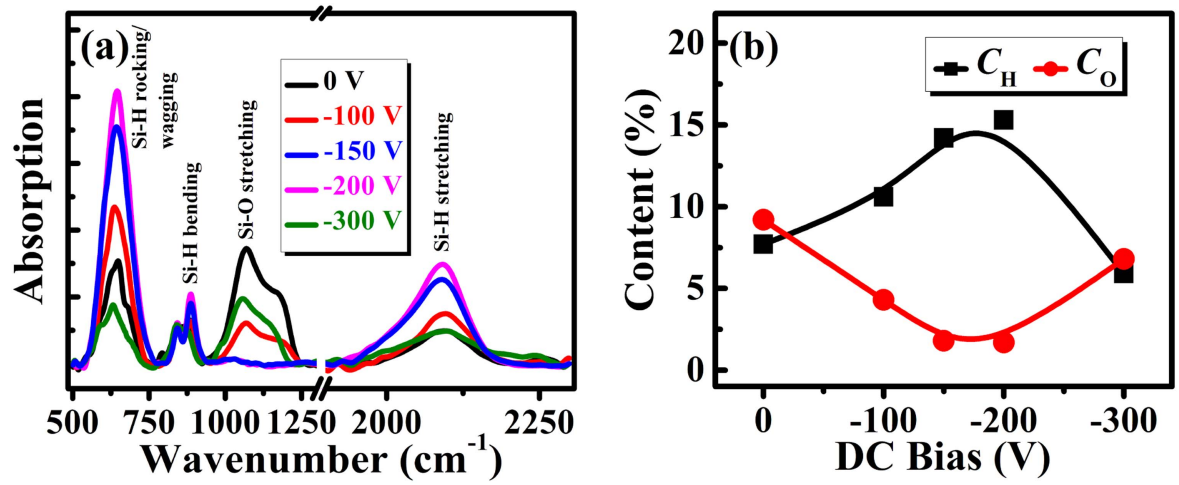

Figure 6. (a) Infrared absorption spectra of nc-Si:H films under various DC biases. (b) Hydrogen and oxygen content of the nc-Si:H films under different DC voltages. Solid lines in (b) are a guide for the eye.

integration of the Si-H rocking/wagging mode at around 640 cm^{-1} using the equation [35, 36]: $C_H = \frac{A_\omega}{N_{Si}} \int \frac{\alpha(\nu)}{\nu} d\nu$, where ν is the wave number, $\alpha(\nu)$ is the absorption coefficient, $A_\omega = 2.1 \times 10^{19}\,cm^{-2}$ is the proportionality constant [35], $N_{Si} = 5 \times 10^{22}\,cm^{-3}$ is the atomic density of crystalline silicon. Analogously, the bonded-oxygen content C_O could be obtained by numerical integration of the Si-O stretching mode at around 1070 cm^{-1} with $A_\omega = 2.8 \times 10^{19}\,cm^{-2}$ [37, 38]. The variations of C_H and C_O with increasing DC bias have been demonstrated in figure 6(b). We can see that C_H increases as the DC bias increases from 0 V to −200 V, and then decreases as the DC bias further increases to −300 V. On the contrary, C_O shows an inverse evolution compared with C_H, which is in good agreement with the SIMS results in figure 2(e). It is worth noting that there is a strong positive correlation between C_H and [P] by contrasting figure 6(b) with figure 2(d). It could be explained by the increasing hydrogen passivation of Si dangling bonds in amorphous matrix [39, 40] and P atoms in Si-NCs. Along with shrinking grain size accompanied with increasing P concentration, more P atoms are incorporated near the surface of the Si-NCs, which are more likely to be passivated by H atoms.

5. Conclusions

P-doped nc-Si:H has been prepared by the PECVD method, applying a tunable substrate DC bias in the range of 0 ~ −300 V. Phosphorus concentration and grain size of the Si-NCs were regulated by the substrate DC bias simultaneously, offering an appropriate way to study the size dependence of phosphorus doping in Si-NCs. Phosphorus concentration was mainly associated with ion bombardment controlled by the substrate DC bias and the difference of bonding energy between the Si-Si bond and P-Si bond. Experimental results demonstrated that grain size varied inversely with phosphorus concentration. Free carrier concentration provided by activated P atoms declined with decreasing grain size. Free carrier concentration depends primarily on the formation energy and activation energy of P atoms incorporated in Si-NCs that both increase with decreasing grain size. Furthermore, our first-principles calculations manifest that most of the P atoms incorporated in Si-NCs prefer to reside near the surface of the Si-NCs and H atoms could passivate P atoms in the form of P-Si-H complex. Hence, the effective doping efficiency of P atoms incorporated in Si-NCs is mainly associated with formation energy, activation energy and hydrogen passivation.

Acknowledgments

This work was supported by the National Natural Science Foundation of China (61234005, 11474201 and 11674225). Wei He would like to thank Dr Limin Sun from Instrumental Analysis Center of Shanghai Jiao Tong University for XPS measurements and Prof Fanying Meng from Shanghai Institute of Microsystem and Information Technology, Chinese Academy of Sciences, for Hall effect measurements.

References

[1] Cantele G, Degoli E, Luppi E, Magri R, Ninno D, Iadonisi G and Ossicini S 2005 First-principles study of *n*- and *p*-doped silicon nanoclusters *Phys. Rev.* B **72** 113303
[2] Dalpian G M and Chelikowsky J R 2006 Self-purification in semiconductor nanocrystals *Phys. Rev. Lett.* **96** 226802
[3] Chan T L, Tiago M L, Kaxiras E and Chelikowsky J R 2008 Size limits on doping phosphorus into silicon nanocrystals *Nano Lett.* **8** 596–600
[4] Melnikov D V and Chelikowsky J R 2004 Quantum confinement in phosphorus-doped silicon nanocrystals *Phys. Rev. Lett.* **92** 046802
[5] König D, Gutsch S, Gnaser H, Wahl M, Kopnarski M, Göttlicher J, Steininger R, Zacharias M and Hiller D 2015 Location and electronic nature of phosphorus in the Si nanocrystal−SiO_2 system *Sci. Rep.* **5** 09702

[6] Stegner A R, Pereira R N, Lechner R, Klein K, Wiggers H, Stutzmann M and Brandt M S 2009 Doping efficiency in freestanding silicon nanocrystals from the gas phase: phosphorus incorporation and defect-induced compensation *Phys. Rev.* B **80** 165326

[7] Sumida K, Ninomiya K, Fujii M, Fujio K and Hayashi S 2007 Electron spin-resonance studies of conduction electrons in phosphorus-doped silicon nanocrystals *J. Appl. Phys.* **101** 033504

[8] Wen C, Xu H, Liu H, Li Z P and Shen W Z 2013 Passivation of nanocrystalline silicon photovoltaic materials employing a negative substrate bias *Nanotechnology* **24** 455602

[9] Lide D R 2010 *CRC Handbook of Chemistry and Physics* 90th edn (Boca Raton, FL: CRC Press/Taylor and Francis)

[10] Hamers E A G, Fontcuberta I Morral A, Niikura C, Brenot R and Roca I Cabarrocas P 2000 Contribution of ions to the growth of amorphous, polymorphous, and microcrystalline silicon thin films *J. Appl. Phys.* **88** 3674–88

[11] Kalache B, Kosarev A I, Vanderhaghen R and Roca I Cabarrocas P 2003 Ion bombardment effects on microcrystalline silicon growth mechanisms and on the film properties *J. Appl. Phys.* **93** 1262–73

[12] Nakamura K, Yoshino K, Takeoka S and Shimizu I 1995 Roles of atomic hydrogen in chemical annealing *Jpn. J. Appl. Phys.* **34** 442–9

[13] Sriraman S, Agarwal S, Aydil E S and Maroudas D 2002 Mechanism of hydrogen-induced crystallization of amorphous silicon *Nature* **418** 62–5

[14] Hao X J, Cho E-C, Flynn C, Shen Y S, Conibeer G and Green M A 2008 Effects of boron doping on the structural and optical properties of silicon nanocrystals in a silicon dioxide matrix *Nanotechnology* **19** 424019

[15] Alpuim P, Chu V and Conde J P 2003 Electronic and structural properties of doped amorphous and nanocrystalline silicon deposited at low substrate temperatures by radio-frequency plasma-enhanced chemical vapor deposition *J. Vac. Sci. Technol.* A **21** 1048–54

[16] Chen H, Gullanar M H and Shen W Z 2004 Effects of high hydrogen dilution on the optical and electrical properties in B-doped nc-Si:H thin films *J. Cryst. Growth* **260** 91–101

[17] Tauc J, Grigorovici R and Vancu A 1966 Optical properties and electronic structure of amorphous germanium *Phys. Stat. Sol.* **15** 627–37

[18] Delley B 1990 An all electron numerical method for solving the local density functional for polyatomic molecules *J. Chem. Phys.* **92** 508–17

[19] Delley B 1990 From molecules to solids with the $DMol^3$ approach 2000 *J. Chem. Phys.* **113** 7756–64

[20] Lee C, Yang W and Parr R G 1988 Development of the Colic-Salvetti correlation-energy formula into a functional of the electron density *Phys. Rev.* B **37** 785–9

[21] Fitzsimmons M R, Eastman J A, Muller-Stach M and Wallner G 1991 Structural characterization of nanometer-sized crystalline Pd by x-ray-diffraction techniques *Phys. Rev.* B **44** 2452–60

[22] Bustarret E, Hachicha M A and Brunel M 1988 Experimental determination of the nanocrystalline volume fraction in silicon thin films from Raman spectroscopy *Appl. Phys. Lett.* **52** 1675–7

[23] Droz C, Vallat-Sauvain E, Bailat J, Feitknecht L, Meier J and Shah A 2004 Relationship between Raman crystallinity and open-circuit voltage in microcrystalline silicon solar cells *Sol. Energy Mater. Sol. Cells* **81** 61–71

[24] Wen C, Xu H, He W, Li Z P and Shen W Z 2014 Tuning oxygen impurities and microstructure of nanocrystalline silicon photovoltaic materials through hydrogen dilution *Nanoscale Res. Lett.* **9** 303

[25] Wang Y J, Chen X X and Hamers R J 1994 Atomic-resolution study of overlayer formation and interfacial mixing in the interaction of phosphorus with Si(001) *Phys. Rev.* B **50** 4534–47

[26] Perego M, Bonafos C and Fanciulli M 2010 Phosphorus doping of ultra-small silicon nanocrystals *Nanotechnology* **21** 025602

[27] Jo M H, Park H H, Kim D J, Hyun S H, Choi S Y and Paik J T 1997 SiO_2 aerogel film as a novel intermetal dielectric *J. Appl. Phys.* **82** 1299–304

[28] Himpsel F J, McFeely F R, Taleb-Ibrahimi A, Yarmoff J A and Hollinger G 1988 Microscopic structure of the SiO_2/Si interface *Phys. Rev.* B **38** 6084–96

[29] Kumar P and Schroeder B 2008 Electrical properties/doping efficiency of doped microcrystalline silicon layers prepared by hot-wire chemical vapor deposition *Thin Solid Films* **516** 580–3

[30] Pi X D, Gresback R, Liptak R W, Campbell S A and Kortshagen U 2008 Doping efficiency, dopant location, and oxidation of Si nanocrystals *Appl. Phys. Lett.* **92** 123102

[31] Johnson N M, Herring C and Chadi D J 1986 Interstitial hydrogen and neutralization of shallow-donor impurities in single-crystal silicon *Phys. Rev. Lett.* **56** 769–72

[32] Chang K J and Chadi D J 1988 Theory of hydrogen passivation of shallow-level dopants in crystalline silicon *Phys. Rev. Lett.* **60** 1422–5

[33] Fukata N, Sato S, Morihiro H, Murakami K, Ishioka K, Kitajima M and Hishita S 2007 Dopant dependence on passivation and reactivation of carrier after hydrogenation *J. Appl. Phys.* **101** 046107

[34] Fukata N, Chen J, Sekiguchi T, Matsushita S, Oshima T, Uchida N, Murakami K, Tsurui T and Ito S 2007 Phosphorus doping and hydrogen passivation of donors and defects in silicon nanowires synthesized by laser ablation *Appl. Phys. Lett.* **90** 153117

[35] Langford A A, Fleet M L, Nelson B P, Lanford W A and Maley N 1992 Infrared absorption strength and hydrogen content of hydrogenated amorphous silicon *Phys. Rev.* B **45** 13367–77

[36] Kroll U, Meier J, Shah A, Mikhailov S and Weber J 1996 Hydrogen in amorphous and microcrystalline silicon films prepared by hydrogen dilution *J. Appl. Phys.* **80** 4971–5

[37] Lucovsky G, Nemanich R J and Knights J C 1979 Structural interpretation of the vibrational spectra of *a*-Si:H alloys *Phys. Rev.* B **19** 2064–73

[38] Freeman E C and Paul W 1978 Infrared vibrational spectra of rf-sputtered hydrogenated amorphous silicon *Phys. Rev.* B **18** 4288–300

[39] Fedders P A 1998 Theory of phosphorus doping in *a*-Si:H *Phys. Rev.* B **58** 7020–3

[40] Pandey A, Cai B, Podraza N and Drabold D A 2014 Electrical activity of boron and phosphorus in hydrogenated amorphous silicon *Phys. Rev. Applied* **2** 054005